Flash sintering of zircon: rapid consolidation of an ultrahigh bandgap ceramic

Juan Manuel Martinez, Mattia Biesuz, Jian Dong, Matias Gauna, Gustavo Suarez, Vincenzo M. Sglavo, Hua-Tay Lin, Salvatore Grasso & Nicolas M. Rendtorff

Published online: 06 Jan 2021.

Submit your article to this journal ↗

View related articles ↗

View Crossmark data ↗

THE CERAMIC SOCIETY OF JAPAN   THE KOREAN CERAMIC SOCIETY   Taylor & Francis
Taylor & Francis Group

FULL LENGTH ARTICLE

Flash sintering of zircon: rapid consolidation of an ultrahigh bandgap ceramic

Juan Manuel Martinez[a,b], Mattia Biesuz[c], Jian Dong[d], Matias Gauna[a,b], Gustavo Suarez[a,b], Vincenzo M. Sglavo[c], Hua-Tay Lin[e], Salvatore Grasso[d] and Nicolas M. Rendtorff[a,b]

[a]CETMIC Centro de Tecnología de Recursos Minerales y Cerámica (CIC-CONICET La Plata), M.B. Gonnet, Buenos Aires, Argentina; [b]Departamento de Química, Facultad de Ciencias Exactas, Universidad Nacional de La Plata, La Plata, Buenos Aires, Argentina; [c]Department of Industrial Engineering, University of Trento, Trento, Italy; [d]Key Laboratory of Advanced Technologies of Materials, Ministry of Education, School of Materials Science and Engineering, Southwest Jiaotong University, Chengdu, China; [e]School of Electromechanical Engineering, Guangdong University of Technology, Guangzhou, China

ABSTRACT

Zircon ($ZrSiO_4$) is a refractory structural ceramic material difficult to consolidate because of its thermal dissociation into ZrO_2 and SiO_2. Addition of sintering aids can improve its densification, but with detrimental effects on high temperature mechanical properties and corrosion resistance. In this work, zircon was consolidated by employing the Flash Sintering (FS) technique at a furnace temperature of 1250°C under an electrical field of 1000 V cm^{-1}. The decomposition of zircon was significantly reduced by lowering sintering time and current density. Unlike conventional sintering methods, FS approach allowed to track the degree of dissociation by measuring the electrical resistivity, providing a promising route for the consolidation of such materials. Although the obtained zircon ceramics are characterized by lower density and hardness/toughness than those sintered by alternative advanced techniques (like SPS of HEBM activated powders), the consolidation can be carried out at remarkably reduced furnace temperature.

1. Introduction

Zircon ($ZrSiO_4$) is a natural occurring mineral with low thermal expansion coefficient (2.5 ppm °C^{-1}), good thermal stability (dissociation temperature of 1673 ± 10°C), and high hardness [1,2], which makes it attractive for high temperature applications in the refractory industry. Other peculiar properties of zircon are its high corrosion resistance to molten slag and glass, as well as its capability to immobilize nuclear wastes, acting as a host for uranium and thorium within its crystal lattice [1,3–6].

Zircon has a high thermodynamic and chemical stability; its natural minerals contain traces of uranium and thorium. Such combination of properties enables its use in geochronology for dating rocks back to 4.5 billion years. It has also a relatively high dielectric constant ($\varepsilon_r = 9.1$) and a large energy gap (6.5–7 eV), enabling its application as a high-κ gate dielectric material in the metal oxide-semiconductor technology [7–9]. In spite of its unique properties, $ZrSiO_4$ is, in general, difficult to sinter due to its high refractoriness and tendency to decompose at elevated temperatures. For conventional sintering, processing temperatures are as high as 1600°C with holding times of at least 2 h [10,11]. If higher temperatures (>1700°C) are used, zircon gradually decomposes into amorphous silica and zirconia (ZrO_2) [1].

Several approaches have been developed to overcome these limitations, such as mechanochemical activation of the powders [11] and the use of advanced sintering techniques such as spark plasma sintering [12,13], hot-pressing [14,15], and microwave-assisted sintering [16]. On the other hand, dense zircon ceramics can be fabricated by incorporating sintering aids [14,17,18], although the addition of such oxides can cause a partial reduction of its properties.

An innovative way to process dense zircon ceramics, never attempted before, could be Flash Sintering (FS) [19]. FS is [20] a current-assisted sintering technology characterized by rapid densification (matter of few seconds-minutes) and by the simultaneous observation of the flash event, including a thermal runaway of internally generated Joule heating, electrical resistivity abrupt drop, and strong bright light emission. Namely, an onset field/temperature combination causes a power surge (the "flash event"), resulting in nearly instantaneous densification of the material [21].

This innovative sintering technique presents several advantages when compared to conventional sintering, such as the reduction of time and costs due to the lower temperatures and shorter sintering times [20,21]. Reduced sintering time and lower furnace temperature have other associated beneficial effects reflected in the fine grained/nanometric microstructure [22], and the consolidation of out-of-equilibrium phases [20,23]. The

---

absence of constrained sintering upon FS makes this technique suitable for the preparation of multilayered and composite ceramics [24].

It is important to remind that the internal heat generation by the Joule effect is one of the main features of this technique [25,26]. Though the initial works on FS were carried out on ionic conductors [19,27], during the last years, materials with far different electrical properties have been sintered with FS technique. Electronic conductors require high currents to produce enough heating to trigger the flash event, and this is typically achieved using flash spark plasma sintering approach without the need for preheating [28–31].

Being the conduction across the sintering material a key parameter to sustain Joule heating, high bandgap materials like zircon are hard to flash sinter because they require the application of very high fields in combination with furnace heating. For instance, high-purity alumina (99.999% pure) cannot be flashed because the internal heat generation by the Joule effect is not high enough to trigger the flash event [32,33].

Zircon, because of its very wide bandgap (and the absence of significant ionic conduction) falls into the latter category of materials, as it presents low conductivity values (4.17×10^{-4} S cm^{-1}) even at temperatures as high as 1478°C [34].

One of the drawbacks of FS is the development of hot-spots during the flash transition due to the electric power spike [35]. These hot-spots can lead to non-homogenous microstructures [36]. In order to reduce hot-spots formation, some authors developed flash processes where the current limit is raised stepwise during the process [37–39].

The aim of this work is to provide insights into the following questions: (i) can zircon be flash sintered despite its low electrical conductivity? (ii) Can we attain a dense microstructure using a current-ramp FS approach? (iii) Which are the main microstructural features of flash sintered zircon?

2. Experimental procedures

Commercial zircon powder (Kreutzonit Super Extra Weiß, Mahlwerke Helmut Kreutz GmbH, Germany) was used in this study. As informed by the manufacturer, it has an average particle size of 0.8 µm and its chemical composition is (wt %): ZrO_2 64–65.5, SiO_2 33–34, Fe_2O_3 ≤ 0.1, Al_2O_3 ≤ 0.1, TiO_2 ≤ 0.15 [40]. The

powder was dispersed in acetone and 1% of polypropylene carbonate binder (QPAC 40, Empower materials, USA) was added. After 24 h drying at room temperature, the resulting powder was grounded by mortar and pestle and then uniaxially pressed at 100 MPa in a heated (40°C) dog-bone shaped die (gage length = 20 mm; cross-section = 3 x 3 mm^2). Then, the samples were presintered at 1200°C in an electric furnace in static air atmosphere. Lower temperatures of 800°C and 1000°C were tried for pre-sintering the dog-bone samples, but the obtained specimen crumbled upon handling to insert the FS electrodes. The relative green density of the samples was 55%, while the green density of the presintered specimen was 57%. For this study, as usual, when using this type of die, only the middle section (i.e. the constant cross-section region of the dog bone) was analyzed.

Flash sintering of the pre-sintered samples was carried out within a tubular furnace (Nabertherm P330) kept at a constant temperature of 1250°C in air atmosphere. Two 90Pt-10Rh wires were forced within the holes on the opposite sides of the dog-bone specimen. Pt paste (C60903P5 Gwent) was spread on the metal/ceramic interface to improve the electric contact. The samples were introduced within the pre-heated furnace and connected to a DC power source (Glassman EW series 5 kV-120 mA). The electric data were recorded at 1 Hz using a Keithley 2100 digital multimeter. Two minutes after the samples had been introduced in the furnace, the flash experiment started. The voltage limit of the power source was set at 1000 V cm^{-1}. The current limit was increased with a step function. Current needed to be gradually increased, otherwise sparks appeared making the flash sintering impossible. Samples were subjected to three different sintering conditions and they were labeled accordingly: (i) low current density values of 4 mA mm^{-2} (L-ZS) with no holding time, (ii) same conditions with 2 min holding time at 4 mA mm^{-2} (LH-ZS) and (iii) high current density of 11 mA mm^{-2} (H-ZS). The sample names are described in Table 1. Materials produced using a single step of current produced arching and are not discussed in this paper.

An estimate of the temperature of the samples upon FS was carried out according to Raj [41] by assuming black body radiation and no temperature gradients across the sample. By equating the electrical power dissipation to the radiative heat loss, the sample temperature (T_s) is obtained as:

Table 1. Current density applied on flash sintered samples. See also Figure 1.

Sample		Step 1	Step 2	Step 3	Step 4	Step 5	Step 6	Step 7	Step 8	Step 9
L-ZS	J [mA mm^{-2}]	1.3	2.6	4	-	-	-	-	-	-
	t [s]	15	15	15	-	-	-	-	-	-
LH-ZS	J [mA mm^{-2}]	1.3	2.6	4	-	-	-	-	-	-
	t [s]	15	15	120	-	-	-	-	-	-
H-ZS	J [mA mm^{-2}]	1.3	2.6	4	5.3	6.6	7	8.3	9.6	11
	t [s]	15	15	15	15	15	15	15	15	15

$$T_S = \left(T_0^4 + \frac{W}{A\varepsilon\sigma} \right)^{1/4} \qquad (1)$$

where T_0 is the furnace temperature, W the power dissipation in the steady stage of FS, A the surface area of the specimen (assumed to be the gauge section), ε the emissivity of the material and σ Stefan and Boltzmann constant. The emissivity value for zircon used in Equation (1)was 0.52 [42].

Manually fracture flash sintered samples were observed using a Leica S APO stereo microscope. X-ray diffraction of sintered samples (Bruker D8 Advanced equipment with Cu Kα in Ni filter at 40 kV to 30 mA, 1 s steps of 0.04° 2θ) was performed at 2θ between 15° and 80°. Apparent density and open porosity of the sintered samples were obtained by the Archimedes' method. Due to the small sample size, at least 10 measurements were taken for each sample.

Further, microstructural analysis of the sintered samples was carried out by Scanning Electronic Microscope (SEM, JEOL JMS-6000, Japan). Samples were mounted in epoxy resin, polished and coated by sputtering with a thin layer of carbon. Back-

Scattered-Electrons (BSE) imaging mode was also used in order to further assess possible dissociation of zircon. Images were taken in the middle section of the dog-bone samples, and estimated values of zircon dissociation were obtained from BSE images, by correlating each phase to its corresponding intensity in the histogram of each image and quantifying zircon across the surface sample. At least five images were analyzed in this way for each sample.

Vickers hardness tests of the sintered samples were conducted with a microindenter (Buehler, USA) using a 3 kg load and 15 s dwell time. At least 10 indentations were produced on each sample.

3. Results and discussion

The flash event was successfully reproduced on zircon. All samples were flash sintered with a current step regulation (CSR) approach. Electrical data (Figure 1) revealed that each current step up was accompanied by a small voltage/field spike, each spike decreasing in height with increasing current. This observed phenomenon is attributed to Ohm's law. The increased
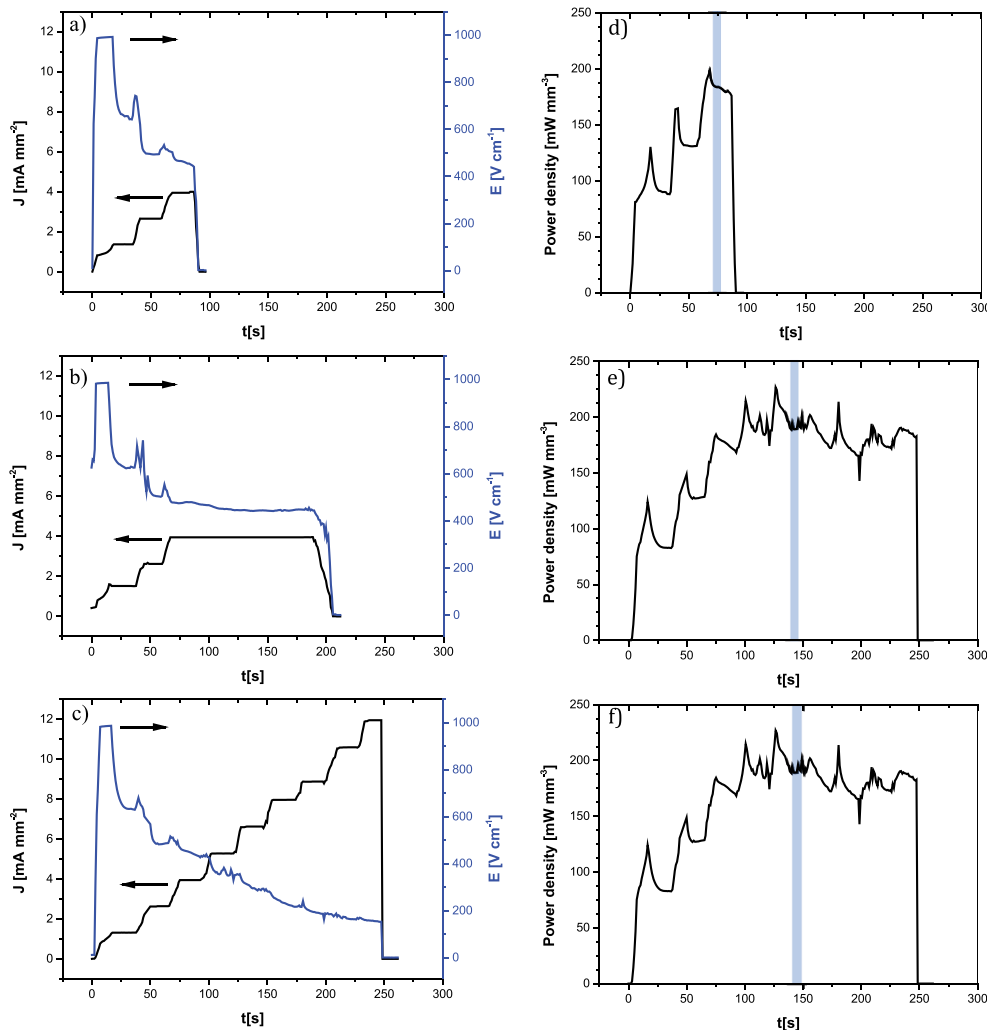
Figure 1. Current density and field vs time for (a) L-ZS (b) LH-ZS (c) H-ZS and power density vs time for (e) L-ZS (f) LH-ZS (g) H-ZS. (sections used for temperature estimation encircled in blue).

electrical conductivity with the temperature promoted the thermal runaway effect [25].

From the electrical data of the flash sintering of the samples, different parameters were obtained, as shown in Table 2. Both L-ZS and LH-ZS samples show similar values of peak power dissipation, temperature and resistivity. Sample H-ZS shows a higher value of peak power dissipation, a slightly higher temperature and a resistivity of an order of magnitude less with respect to the other samples. Zircon can undergo partial dissociation at high temperatures, being ZrSiO$_4$ the major stable phase up to ~1500°C [11,13], according to the following reaction:

$$ZrSiO_4 \leftrightarrow (monoclinic - tetragonal)ZrO_2 + SiO_2(amorphous) \qquad (2)$$
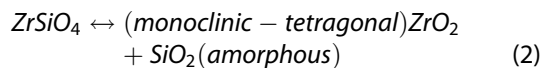
Both purity and grain size strongly influence the onset temperature for zircon dissociation [1]. Sample H-ZS was subjected to FS for a longer period at high temperature, which presumably can account for a larger degree of dissociation with respect to L-ZS and LH-ZS. This higher degree of dissociation could also explain the drop in resistivity at the end of the process in sample H-ZS, as ZrSiO$_4$ electrical resistivity at high temperatures is higher than that of silica glass and ZrO$_2$.

The surface of the samples was observed (Figure 2 (b)) revealing a highly cracked structure in sample H-ZS, while macroscopic cracks were absent in samples L-ZS and LH-ZS. Thermal shock (abrupt temperature gradients) together with decomposition and thermal expansion mismatch of the ZrO$_2$-SiO$_2$ -ZrSiO$_4$ phases might explain the crack formations in sample H-ZS.

The cross-section of the anode and cathode region is also shown, revealing a blackening in the center of samples L-ZS and H-ZS. This effect could be another indication of a partial dissociation of zircon into silica and ZrO$_2$ phases (Equation (2)), with the electrochemical blackening of ZrO$_2$-like phases being responsible for such behavior as discussed in [43] and [44].

As explained in previous works, blackening develops from the cathode and moves toward the anodic region, analogously to the well-known electrochemical blackening associated with the partial reduction of ZrO$_2$ [45]. This black "core" surrounded by a white surface layer is explained by the rapid re-oxidation of the surface upon cooling after FS.

The blackening phenomena is certainly of interest to understand the flash sintering mechanisms. As
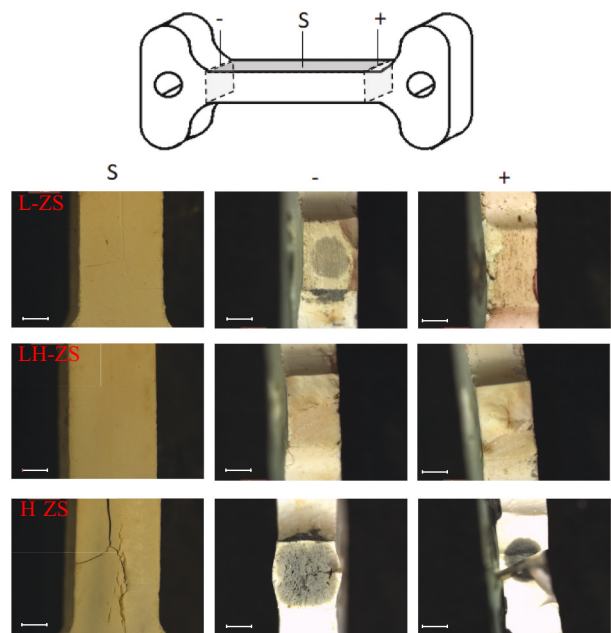

Figure 2. Schematic representation of dog-bone samples; and (b) Stereoscopic microscope images of the flash sintered samples external surface (S) and of their cross-sections close to the cathode (-) and anode (+). (scale bar 1 mm).

summarized in Table 2, the blackening can be qualitatively associated with the electrical resistivity of the sample. The lower the sample resistivity, the more significant is the blackening. LH-ZS material was heavily blackened because of the high current density (11 mA/mm^2) and the final resistivity of 1.28 kΩ cm. For samples L-ZS and LH-ZS, the blackening effect was rather mild and the sample resistivity at the end of FS was in both cases 11.3 kΩ cm. To be more precise, L-ZS sample was more blackened and more prone to cracking than sample LH-ZS (Figure 2). The latter effect can be explained by looking at the power profiles (Figure 1) The L-ZS sample reached a powder dissipation of 200 mw/mm^3 after 70 s while 110 s was needed for the LH-ZS. The smooth LH-ZS raise in power might justify the absence of cracking and blackening. The current and power
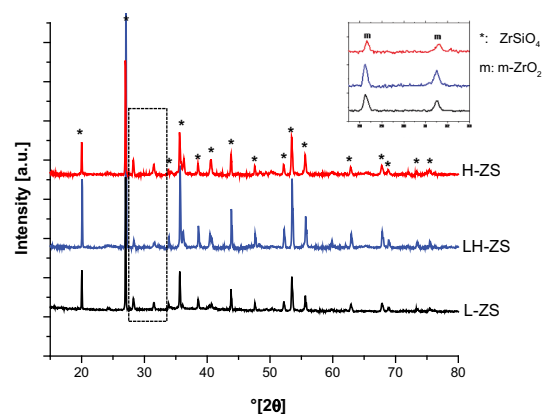

Figure 3. XRD plots of solid sintered dog-bone samples Inset: m-ZrO$_2$ peaks.

Table 2. Parameters calculated from electrical data collected during FS experiments.

Sample	L-ZS	LH-ZS	H-ZS
Peak power dissipation [mW mm3]	198.3	191.7	226.7
Temperature [°C]*	1506	1512	1520
Resistivity at the end of the process [kΩ cm]	11.3	11.3	1.28
Electrical discharge time [s]	90	200	245

Table 3. Open porosity and apparent density of ZrSiO₄ flash sintered samples (the error corresponds to the standard deviation).

Sample	L-ZS	LH-ZS	H-ZS
Apparent density [g/cm^3]	3.91 ± 0.08	3.96 ± 0.14	3.73 ± 0.12
Open porosity [%]	<1.5	<1	<4
Cracking	Yes, minor	No	Yes, extensive

increase effects in FS are particularly important and they have been discussed in [46]

Figure 3 shows XRD plots of the sintered zircon samples. Interestingly, although not all samples blackened, there is a degree of dissociation in all of them, evident by the presence of monoclinic ZrO₂ (m-ZrO₂) peaks. Although the ZrO₂ formed by partial dissociation of zircon is usually tetragonal ZrO₂ (t-ZrO₂, in agreement with its thermodynamic stability range) it can transform spontaneously to m-ZrO₂ at room temperature [1,13,47,48]. Besides ZrSiO₄ and m-ZrO₂, no other crystalline phases were found, thus confirming that the SiO₂ derived from the dissociation went into an amorphous (glassy) phase. Samples were later exposed to thermal annealing at 800°C for 1 h and XRD measurements do not reveal any other crystalline phases, thus confirming that the blackening of the samples was attributable to ZrO₂ partial reduction [45].

Table 3 reports the apparent density and open porosity of the samples. Due to the small size of the samples, open porosity values show a large scatter, even after 10 measurements. As such, only upper threshold values are shown. All samples show an open porosity below 4%. The highest apparent density was found in samples L-ZS and LH-ZS.

There is a decrease in density with increasing current (Table 1), this being an unusual effect in flash sintering since higher current usually leads to Joule effect heating and sintering. Although low open porosity values were found, in general, apparent density is quite lower than zircon theoretical density (4.65 g cm^{-3}), with H-ZS material showing the lowest value.

Possible explanations for these effects could be a combination of closed porosity and partial decomposition of zircon. As stated before (Equation (2)), the products of the reaction are amorphous silica glass (density 2.2 g cm^{-3}) and either m-ZrO₂ or t-ZrO₂ (density equal to 5.83 and 6.10 g cm^{-3}, respectively), which give a total theoretical density of the products between 3.78 and 3.87 g cm^{-3}, this value being dependent on the type of ZrO₂ phase formed. The products of the reaction give a total theoretical density lower than that of pure ZrSiO₄, which explains the lower densities.
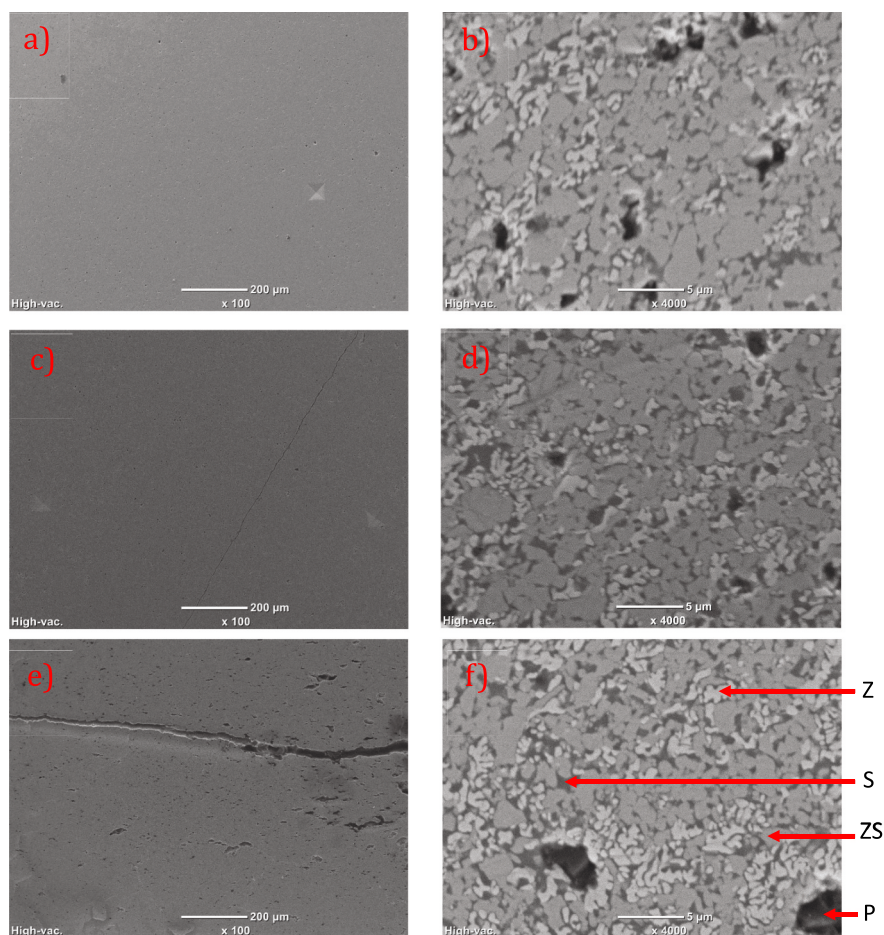

Figure 4. SEM (BSE) images of FS samples (a,b) L-ZS (c,d) LH-ZS and (e,f) H-ZS . (P: Pores, Z: ZrO₂, ZS: ZrSiO₄, S: SiO₂). Palmqvist indents can be observed in images (a) and (c).

SEM micrographs taken on samples L-ZS (Figure 4(a, b)) and LH-ZS (c,d) show a homogeneous microstructure, low porosity and minor or no defects, while a non-homogeneous microstructure filled with cracks and defects is revealed in sample H-ZS (Figure 4(e,f)).

The dissociation in samples LH-ZS and H-ZS was comparatively higher than in sample L-ZS, as seen by the presence of higher amounts of ZrO_2 (light gray) and silica (dark gray) derived from this reaction. Also, the presence of porosity in all samples not revealed by the Archimedes' method further suggests that this closed porosity is derived from defects originated upon sintering.

From SEM images and considering the distinct color of each phase present, analysis of the histogram of the images yields an estimate of zircon's degree of decomposition in each sample, as shown in Table 4. For this calculation, the theoretical density of each phase was considered and the mass fraction was calculated accordingly. As expected, decomposition rate increases with temperature and sintering times.

Table 4 shows the measured Vickers hardness for samples L-ZS and LH-ZS. High current values in sample H-ZS (associated with an overheating of the samples) produced a much weaker structure, as samples tended to crack when handled. As such, Vickers hardness was not measured for this sample. Vickers hardness is slightly lower for sample LH-ZS when compared with sample L-ZS. Gauna et al. [11] well correlated the hardness of different zircon samples with their densities. As explained before, zircon's dissociation brings about a decrease in density, which explains the obtained values when compared to those obtained on fully sintered materials. With the aim to compare the obtained results with the literature, the relative density of the sintered samples was calculated against zircon theoretical density, giving values of 83% and 85% for LH-ZS and L-ZS, respectively. The comparison is shown in Table 5.

In Table 5, a comparison is made between the zircon material sintered in the present study and those reported in the literature. Vickers hardness of flash sintered samples is comparable to values found in previous works on materials with similar density [11,52], although lower than those found in the literature for dense zircon ceramics produced by SPS or hot pressing. In spite of the obtained lower density and hardness, FS technique allows to consolidate zircon at a much lower furnace temperature. The resulting open porosity is well below 1.5%, value only obtained with

Table 4. Vickers hardness of $ZrSiO_4$ sintered samples. (the error corresponds to the standard deviation).

Sample	L-ZS	LH-ZS	H-ZS
HV [GPa]	7.55 ± 0.31	6.88 ± 0.40	-
Degree of dissociation [mass %]	39	43	55
Theoretical density accounting for dissociation[g/cm³]	4.16	4.11	3.96
Relative density [%]	94.0 ± 1.92	96.4 ± 3.40	94.2 ± 3.03

Table 5. Comparison of processing parameters and material properties with the data reported in the literature.

Techniques	Maximum temperature, holding time and pressure	Heating rate [°C min]	Relative density [%]	Dissociation	Open porosity [%]	Vickers hardness [GPa]
Conventional sintering with additives [17]	1550°C, 1 h, presureless	15	89–92	Yes	5–10	-
Conventional sintering without additives [10,11]	1615°C, 48 h, pressureless; 1400–1600°C, 2 h	5	92/74-94	Yes	8–12	4–5.5
Sol gel, conventional sintering [49]	1700°C, 4 h, Pressureless	3.33	98	Not informed	Not reported	-
Slip casting, conventional sintering [50]	1600–1680°C, 2 h, pressureless	5	92–94	Yes	Not reported	8.5–8.6
Cold isostatic presssing of pure nanosized SiO_2–ZrO_2 powders, Conventional sintering [51]	1500°C; 4 h; Pressureless	10	99.7	Complete formation	Not reported	-
Mechanochemical activation of the powder, conventional sintering [11]	1400–1600°C, 2 h, Pressureless	5	95%	Yes	<1%	9
Spark Plasma Sintering [52]	1300, 1 h, presureless		82.79	Yes	Not reported	6.7
Mechanochemical activation of the powder, Spark Plasma Sintering [13]	1400°C, 10 min, 100 MPa	100	≈99.5	No	<1	11.4–13.7,
Microwave assisted sintering [16]	1460°C, 1 h, Pressureless	~84	87.6	Yes	11	-
Hot pressing of pure zircon powders [15]	1600°C; 1 h; 25 MPa	Not given	99.1	Yes	Not reported	10
Flash sintering of commercial zircon powders (Present study)	Electric discharge time of 90 s	1250°C	83	Yes	<1.5	7.55
Flash sintering of commercial zircon powders (Present study)	Electric discharge time of 200 s	1250°C	85	Yes	<1	6.88

*Knoop hardness.

advanced techniques such as SPS of mechanochemical activated powders.

4. Conclusions

- Zircon samples were successfully flash sintered by a current ramp regulation approach.
- Flash sintered zircon samples show a variable degree of dissociation and moderate Vickers hardness. Although the relative density is low, the open porosity is small.
- Higher current and longer sintering time cause a higher dissociation of zircon into m-ZrO_2 and SiO_2.

Although completely dense, single-phase materials were not obtained. This work reports the potential path not only for the study of flash sintering of zircon, but also to other high bandgap materials by using a stepwise current increase to avoid the formation of undesired electrical arcs.

Disclosure statement

No potential conflict of interest was reported by the authors.

References

[1] Kaiser A, Lobert M, Telle R. Thermal stability of zircon (ZrSiO4). J Eur Ceram Soc. 2008;28(11):2199–2211.
[2] Xiang H, Feng Z, Li Z, et al. Theoretical investigations on mechanical and thermal properties of MSiO 4 (M= Zr, Hf). J Mater Res. 2015;30(13):2030–2039.
[3] Comstock GF. Some experiments with Zircon and Zirconia refractories. J Am Ceram Soc. 1933;16(1-12):12–35.
[4] Ewing RC, Lutze W, Weber WJ. Zircon: A host-phase for the disposal of weapons plutonium. J Mater Res. 1995;10(2):243–246.
[5] Gediga J, Morfino A, Finkbeiner M, et al. Life cycle assessment of zircon sand. Int J Life Cycle Assess. 2019;24(11):1976–1984.
[6] Rendtorff N, Garrido L, Aglietti E. Mullite–zirconia–zircon composites: properties and thermal shock resistance. Ceram Int. 2009;35(2):779–786.
[7] Chiker F, Boukabrine F, Khachai H, et al. Investigating the structural, thermal, and electronic properties of the Zircon-Type ZrSiO4, ZrGeO4 and HfSiO4 compounds. J Electron Mater. 2016;45(11):5811–5821.
[8] Rignanese GM, Detraux F, Gonze X, et al. Dielectric constants of Zr silicates: a first-principles study. Phys Rev Lett. 2002;89(11):117601.
[9] Wilk GD, Wallace RM. Stable zirconium silicate gate dielectrics deposited directly on silicon. Appl Phys Lett. 2000;76(1):112–114.
[10] Carbonneau X, Hamidouche M, Olagnon C, et al. High temperature behaviour of a zircon ceramic. Key Eng Mater. 1997;132(136):571–574.
[11] Gauna MR, Conconi MS, Suarez G, et al. Dense zircon (ZrSiO4) ceramics by a simple milling-sintering route. Sci Sintering. 2018;50(1):15–28.
[12] Nakamori F, Ohishi Y, Muta H, et al. Mechanical and thermal properties of ZrSiO4. J Nucl Sci Technol. 2017;54(11):1267–1273.
[13] Rendtorff NM, Grasso S, Hu C, et al. Dense zircon (ZrSiO4) ceramics by high energy ball milling and spark plasma sintering. Ceram Int. 2012;38(3):1793–1799.
[14] Huang S, Li Q, Wang Z, et al. Effect of sintering aids on the microstructure and oxidation behavior of hot-pressed zirconium silicate ceramic. Ceram Int. 2017;43(1,Part A):875–879.
[15] Shi Y, Huang X, Yan D. Fabrication of hot-pressed zircon ceramics: mechanical properties and microstructure. Ceram Int. 1997;23(5):457–462.
[16] Ebadzadeh T, Valefi M. Microwave-assisted sintering of zircon. J Alloys Compd. 2008;448(1):246–249.
[17] Awaad M, Kenawy SH. Sintering of zircon: the role of additives. Br Ceram Trans. 2003;102(2):69–72.
[18] Rendtorff NM, Grasso S, Hu C, et al. Zircon–zirconia (ZrSiO4–ZrO2) dense ceramic composites by spark plasma sintering. J Eur Ceram Soc. 2012;32(4):787–793.
[19] Cologna M, Rashkova B, Raj R. Flash sintering of Nanograin Zirconia in <5 s at 850°C. J Am Ceram Soc. 2010;93(11):3556–3559.
[20] Biesuz M, Sglavo VM. Flash sintering of ceramics. J Eur Ceram Soc. 2019;39(2–3):115–143.
[21] Raj R. Analysis of the power density at the onset of flash sintering. J Am Ceram Soc. 2016;99(10):3226–3232.
[22] Perez-Maqueda LA, Gil-Gonzalez E, Perejon A, et al. Flash sintering of highly insulating nanostructured phase-pure BiFeO3. J Am Ceram Soc. 2017;100(8):3365–3369.
[23] Yu JH, McWilliams BA, Parker TC. Densification behavior of flash sintered boron suboxide. J Am Ceram Soc. 2018;101(11):4976–4982.
[24] Jha SK, Raj R. Electric fields obviate constrained sintering. J Am Ceram Soc. 2014;97(10):3103–3109.
[25] Todd RI, Zapata-Solvas E, Bonilla RS, et al. Electrical characteristics of flash sintering: thermal runaway of Joule heating. J Eur Ceram Soc. 2015;35(6):1865–1877.
[26] Zhang Y, Jung J-I, Luo J. Thermal runaway, flash sintering and asymmetrical microstructural development of ZnO and ZnO–Bi2O3 under direct currents. Acta Materialia. 2015;94:87–100.
[27] Muccillo R, Kleitz M, Muccillo ENS. Flash grain welding in yttria stabilized zirconia. J Eur Ceram Soc. 2011;31(8):1517–1521.
[28] Grasso S, Saunders T, Porwal H, et al. Flash spark plasma sintering (FSPS) of pure ZrB 2. J Am Ceram Soc. 2014;97(8):2405–2408.
[29] Manière C, Lee G, Olevsky EA. All-materials-inclusive flash spark plasma sintering. Sci Rep. 2017;7(1):15071.
[30] Manière C, Riquet G, Marinel S. Dielectric properties of flash spark plasma sintered BaTiO3 and CaCu3Ti4O12. Scr Mater. 2019;173:41–45.
[31] McKinnon R, Grasso S, Tudball A, et al. Flash spark plasma sintering of cold-Pressed TiB2-hBN. J Eur Ceram Soc. 2017;37(8):2787–2794.
[32] Biesuz M, Sglavo VM. Flash sintering of alumina: effect of different operating conditions on densification. J Eur Ceram Soc. 2016;36(10):2535–2542.
[33] Cologna M, Francis JSC, Raj R. Field assisted and flash sintering of alumina and its relationship to conductivity and MgO-doping. J Eur Ceram Soc. 2011;31(15):2827–2837.

[34] Wallace RW, Ruh E. Electrical resistivity of refractories. J Am Ceram Soc. 1967;50(7):358–364.

[35] Dong Y. On the hotspot problem in flash sintering. arXiv: Materials Science. 2017.

[36] Campos JV, Lavagnini IR, Silva JG, et al. Flash sintering scaling-up challenges: influence of the sample size on the microstructure and onset temperature of the flash event. Scr Mater. 2020;186:1–5.

[37] Biesuz M, Sglavo VM Field assisted sintering of silicate glass-containing alumina. In: Advanced Processing and Manufacturing Technologies for Nanostructured and Multifunctional Materials II: A Collection of Papers Presented at the 39th International Conference on Advanced Ceramics and Composites. Hoboken, NJ, USA: John Wiley & Sons, Ltd; 2015. p. 75–81.

[38] Kumar MKP, Yadav D, Lebrun J-M, et al. Flash sintering with current rate: A different approach. J Am Ceram Soc. 2019;102(2):823–835.

[39] Lavagnini R I, Campos JV, Ferreira JA, et al. Microstructural evolution of 3YSZ flash-sintered with current ramp control. J Am Ceram Soc. 2020;103 (6):3493–3499.

[40] Gauna MR, Rendtorff NM, Conconi MS, et al. Fine zircon (ZrSiO4) powder mechanical activation, a Perturbed Angular Correlation (PAC) analysis. Ceram Int. 2017;43(15):11929–11934.

[41] Raj R. Joule heating during flash-sintering. J Eur Ceram Soc. 2012;32(10):2293–2301.

[42] Veazey WR, Hodgman CD. Handbook of chemistry and physics. Vol. 7. Chemical Rubber Publishing Company, Boca Raton, Florida; 1919.

[43] Biesuz M, Pinter L, Saunders T, et al. Investigation of electrochemical, optical and thermal effects during flash sintering of 8YSZ. Materials. 2018;11(7):1214.

[44] Grimley CA, Prette ALG, Dickey EC. Effect of boundary conditions on reduction during early stage flash sintering of YSZ. Acta Materialia. 2019;174:271–278.

[45] Sinhamahapatra A, Jeon J-P, Kang J, et al. Oxygen-deficient Zirconia (ZrO2−x): a new material for solar light absorption. Sci Rep. 2016;6(1):27218.

[46] Grimley CA, Funni S, Green C, et al. Perspective of flash sintering: the effect of AC current ramp rate on microstructure evolution. J Eur Ceram Soc. 2020. DOI:10.1016/j.jeurceramsoc.2020.11.040

[47] Garvie RC. Stabilization of the tetragonal structure in zirconia microcrystals. J Phys Chem. 1978;82(2):218–224.

[48] Gupta TK, Bechtold JH, Kuznicki RC, et al. Stabilization of tetragonal phase in polycrystalline zirconia. J Mater Sci. 1977;12(12):2421–2426.

[49] Mori T, Yamamura H, Kobayashi H, et al. Preparation of high-purity ZrSiO4 powder using sol–gel processing and mechanical properties of the sintered body. J Am Ceram Soc. 1992;75(9):2420–2426.

[50] Suárez G, Acevedo S, Rendtorff NM, et al. Colloidal processing, sintering and mechanical properties of zircon (ZrSiO4). Ceram Int. 2015;41(1,Part B):1015–1021.

[51] Tartaj P. Zircon formation from nanosized powders obtained by a reverse micelle process. J Am Ceram Soc. 2005;88(1):222–224.

[52] Anjali MC, Biswas P, Chakravarty D, et al. Low temperature in-situ reaction sintering of zircon: alumina composites trough spark plasma sintering. Sci Sintering. 2012;44(3):323–330.